published in Relaxation Phenomena: Liquid Crystals, Magnetic Systems, Polymers, High-Tc ; Springer-Verlag 2003

Computer Simulations of Polar Liquid Crystals

Lech Longa[1], Hans- Rainer Trebin[2], and Grzegorz Cholewiak[1]

[1] *M. Smoluchowski Institute of Physics, Jagellonian University ul. Reymonta 4, 30-059 Kraków, Poland*

[2] *Institut für Theoretische und Angewandte Physik, Universität Stuttgart Pfaffenwaldring 57, D-70550 Stuttgart, Germany*

1 Introduction

Liquid crystals are condensed matter structures which occur quite frequently in nature [1,2]. But the relationship between molecular interactions and relative stability of the corresponding liquid crystalline phases is still not fully understood. While it is widely accepted that the origin of liquid crystals rests in the elongated or flat or generally anisotropic shape of the molecules experiment and theory clearly show the importance of dispersive, induction and electrostatic interactions. Among them are the interactions between strong dipolar groups of particular interest. This has become evident soon after Gray *et al.* performed the synthesis of cyanobiphenyles [3,4]. In these mesogens, a new class of phenomena known as reentrant phase transitions [5] was discovered and studied over the whole decade [6–8]. Also they appeared important in liquid crystal based display technology. Subsequently, strong dipoles were shown to affect not only the relative stability and the range of liquid crystalline phases, but also their symmetry [1,9–11].

Interesting orderings can also be realized when dipole-dipole interactions are competing with entropy of packing as induced by molecular shape asymmetry. Such a situation is realized *e.g.* in the case of smectic phases formed by banana-shaped liquid crystalline molecules [12–14].

A direct and reliable way to account for structures that could be induced by dipolar forces is offered by computer simulations [15,16]. They provide exact information about molecular ordering that results from particular molecular interactions. A purpose of this chapter is to discuss the effect of dipolar forces on mesophase formation and stability as derived from computer simulations. We are going to concentrate on effects that result from such forces by studying relatively simple models for which the case of a vanishing dipole is understood, too. In particular we shall be concerned with hard-rod and prolate Gay-Berne like molecules with embedded dipole moments for which many

detailed simulations have been reported in the literature. The stability of various liquid crystals as function of position, orientation, molecular shape and strength of the dipole moment will be discussed whenever possible. Emphasis is put on the role that correlation functions play in a proper understanding of the structures and of their local, dipolar organization. Finally, an attempt is made to make the chapter selfcontained by clarifying the essential points associated with the study of dipolar systems. However, we do not intend to give an exhaustive presentation of all known liquid crystalline phases with dipolar ordering. Our choice restricts to those cases that have been accessed in computer simulations, or are relevant to their understanding.

2 Liquid crystalline phases and dipolar ordering.

Of all liquid crystalline phases the simplest one is the uniaxial nematic phase of calamitic liquid crystals. There the long range positional ordering of the centers of mass of the particles is absent and the correlations between the centers of mass of the molecules are similar to those existing in conventional liquids. The long axes of the molecules, on the other hand, lie on average parallel to each other defining a microscopically preferred direction, the *director*. Usually it is denoted by a unit vector $\hat{\mathbf{n}}$.

Though the constituent molecules may be polar, no ferroelectric nematics have been found experimentally so far in low molar mass liquid crystals. Microscopically this means that each molecule points *"up"* or *"down"* with equal probability and, consequently, the directions $\hat{\mathbf{n}}$ and $-\hat{\mathbf{n}}$ are equivalent. A typical snapshot of the molecular configuration is shown in Fig. 1a. However, the existence of a uniaxial polar nematic (which would be a ferroelectric fluid with a macroscopic dipole moment) is not forbidden by symmetry (see Fig. 1b). Actually it has been observed in computer simulations [17,18] and in polymeric systems [19].

More organized structures that could acquire some kind of polar ordering are smectics where the molecules are arranged in equidistant layers. Inside each layer the centers of mass may show no long-range positional order in which case each layer is a two-dimensional liquid. The molecules are, on the average, ordered perpendicular to the layer, as in the smectic A phase, or are tilted. In general, intra-layer diffusion of the molecules is easier than inter-layer. If an extra long-range positional order exists inside the layers such smectics are often referred to as crystal smectics.

The simplest of the smectic phases is the uniaxial smectic A phase of calamitics, which is shown in Fig. 2a. Note that the long molecular axes are, on the average, parallel to the layer normal and the dipoles (if present) are disordered to make the net macroscopic polarization vanish. The layer structure is rather weak and has a periodicity comparable to the length of a molecule in its fully extended configuration.

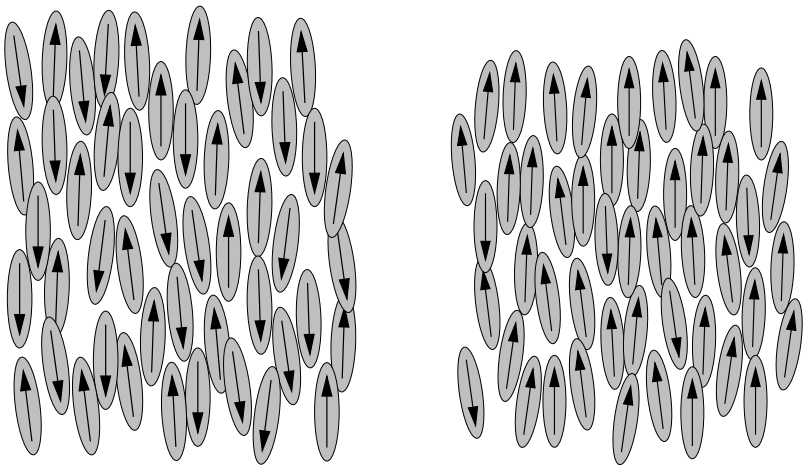

(**a**) (**b**)

Fig. 1. Snapshot of molecular arrangement in (**a**) uniaxial nematic phase composed of polar molecules and (**b**) uniaxial polar nematic phase of rod-like molecules. Arrows indicate orientation of dipole moments. In the case (**a**) the average performed over snapshots cancels out the dipole moment locally

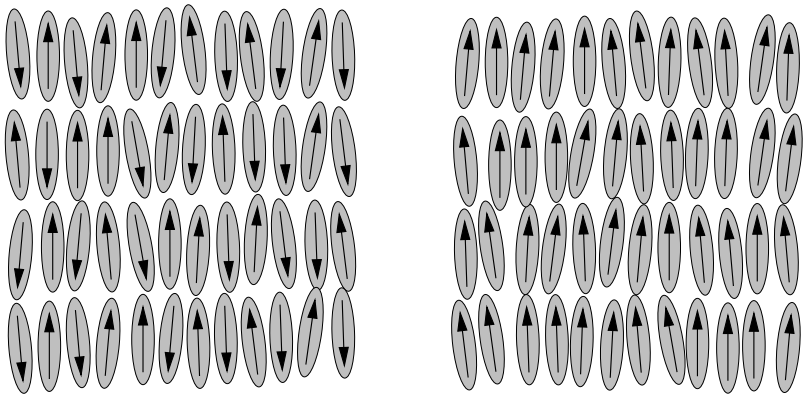

(**a**) (**b**)

Fig. 2. Snapshot of the molecular arrangement in (**a**) a uniaxial, nonpolar smectic A phase and (**b**) a uniaxial polar smectic A phase of rod-like molecules. Arrows indicate the orientation of dipole moments. The average performed over snapshots (**a**) cancels out the dipole moment

As in the case of nematics the existence of a uniaxial polar smectic A phase (Fig. 2b) is not forbidden by symmetry and, indeed, was found in computer simulations of pear-shaped molecules with embedded axial dipole [18]. As far as we are aware of, it has not yet been detected in thermotropic or lyotropic liquid crystals, but films of more than a hundred layers stacked

in a polar arrangement have been found to form by self-assembled mushroom shaped nanostructures of miniaturized triblock copolymers [20].

Another class of orthogonal smectic phases with polarized layers exists in liquid crystal compounds consisting of molecules with a strongly polar cyano- or $\mathcal{NO}_2$ group at the one end of the aromatic core and only a single paraffin tail at the other [1,9,10]. The smectic layers have a thickness ranging from one to two molecular lengths and one observes phase transitions between the optically identical smectic A phases. Out of these phases the so called smectic A_d, Fig.(3a), is similar to classical smectic A. One of the differences is that its periodicity is greater than the molecular length by a factor ranging from 1.1 to 1.6, with a typical value of 1.4. In the smectic A_2 phase, Fig.(3b), each

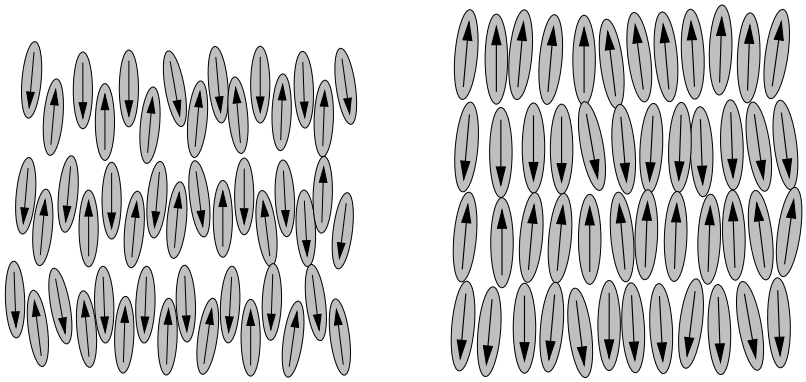

(**a**) (**b**)

Fig. 3. (**a**) Molecular arrangement and dipolar ordering in the uniaxial, smectic A_d phase with cross section parallel to the layer normal. (**b**) Schematic representation of antiferroelectric order in the smectic A_2 phase with cross section parallel to the layer normal. Arrows indicate the orientation of dipole moments

layer has a periodicity comparable to the molecular length but, contrary to the layers of ordinary smectic A phases, it is ferroelectric. The ferroelectricity alternates on going from one layer to the next yielding an overall vanishing macroscopic polarization and antiferroelectric ordering (double layer structure).

A very interesting molecular arrangement is observed in the smectic $\tilde{A}$ phase, also known as 'antiphase', which has been detected both experimentally [10] and in computer simulations [18]. Locally the phase is similar to the smectic A_2, but globally antiferroelectric smectic A_2 domains are observed. They are arranged in a two-dimensional centered, rectangular lattice as shown in Fig.(4a). Thus the polarization of a single sublayer vanishes. If the lattice is assumed to be formed in the (x, z)-plane, the liquid character of the phase is maintained only in the y-direction.

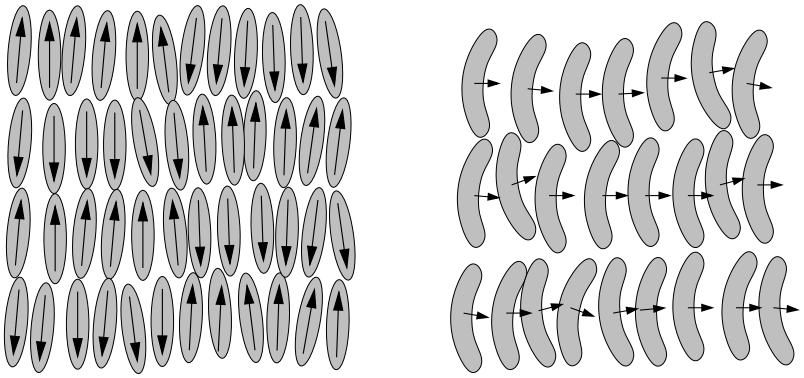

(**a**) (**b**)

Fig. 4. (**a**) Molecular arrangement and dipolar ordering in the smectic $\tilde{A}$ phase with cross section parallel to the layer normal. (**b**) Schematic representation of ferroelectric order in the biaxial smectic A phase formed by banana-shaped molecules with cross section parallel to the layer normal. Arrows indicate orientation of dipole moments

Interestingly, the general rule that the lower temperature phases must display a greater degree of long range order does not always hold for this class of strongly polar liquid crystals. For example, the nematic state could be observed not only at temperatures above the domain of the smectic phase, but also below [5–8]. This behavior is now referred to as reentrant phase transition. Also one is able to observe phase transitions between the optically identical smectic A phases [8–11].

A new type of (anti-) ferroelectric ordering could be predicted for systems where the entropy of packing of molecules within layers is competing strongly with dipolar interactions. This is exactly what we observe for systems of banana-like shaped molecules, where a biaxial, ferroelectric, smectic A phase is formed with spontaneous polarization perpendicular to the layer normal [21], Fig.(4b). On the other hand, discotic molecules with the dipole moments parallel to the rotation axis like to form polarized columns [22] or polar domains within the columns [23]. The overall resulting columnar structure is, however, nonpolar.

Finally, we mention that there exist tilted smectic phases of practical importance, with more complex types of polar ordering. They are not discussed here as we are not aware of any computer simulations relevant to them. Detailed information about their structure is given in [1,24]. Interesting thoughts about liquid crystalline phases with polar order are found in an article by Blinov [25].

3 Models of interacting liquid crystalline molecules

It is obvious that the stability of a given liquid crystalline ordering is a direct consequence of intermolecular interactions. But it is also clear that the use of realistic many-body potentials in computer simulations at nonzero temperatures is an enormously complex computational problem. We therefore are forced to use relatively simple models, which only partly account for known properties of real liquid crystalline molecules. Fortunately, it proves satisfactory for studying gross features of liquid crystalline phases and of their long-range organization. An advantage of such modelling is that it can pinpoint the molecular features that should be looked for in realistic systems to produce a given type of ordering. Our intention in this section is to introduce one of the most successful pair interaction potentials used to study mesophases by means of computer simulations, *the Gay-Berne potential*.

But before we are going to discuss properties of this model we summarize characteristic features of interactions between an arbitrarily shaped, but isolated, pair of molecules. The system is assumed to be in its quantum mechanical ground state. This approach promises a better understanding of what is actually disregarded in the original model and in which direction it could be generalized. Clearly, a restriction to pair interactions is already an approximation to more elaborated approaches in which the total electrostatic interaction between an ensemble of molecules is taken into account by use of the full apparatus of quantum statistical mechanics.

3.1 Pair potentials for liquid crystalline molecules

Under the restrictions discussed above the pair interaction for two isolated molecules can generally be written as the quantum mechanical average of the electrostatic interaction operator over the ground state of the system. However, a detailed analysis of such expression is quite complicated (if not impossible) and further simplifying assumptions are necessary (*see e.g.* [26] *and references therein*). One of them is that the flexibility of the molecules is of secondary importance. Then it simply follows that:

- *at large intermolecular separations the potential must vanish;*
- *at short distances, the overlap of the electron clouds results in a strong repulsion. Though in general interactions at short distances are non-additive (due to electronic exchange effect) often a good approximation of the repulsive part is obtained by treating the molecules as hard bodies*[1].

At short distances the hard body model introduces a simple characteristic of a molecular system, the so called *packing fraction*. It is defined as the ratio of the molecular ("Van der Waals") volume to the average volume

[1] By definition a hard body is impenetrable when in contact with another hard body but otherwise do not interact.

per particle (as calculated from the density number). For example, cylinders closely packed in a hexagonal lattice yield a packing fraction $\frac{\pi}{2\sqrt{3}} \approx 0.906$. The experimentally found packing fraction for high temperature liquid crystalline phases is of the order of 0.66. For an ensemble of strongly elongated molecules it results in a tendency towards *parallel* ordering of long molecular axes (entropic excluded volume effects).

At another extreme, *i.e.* for large intermolecular separations, the overlapping of electronic clouds can be disregarded and thus the complete single-molecule bases can be used to decompose the ground state of the two molecules. The resulting expression yields three classes of terms

- **The electrostatic energy**. It is the electrostatic interaction between two separated, generally inhomogeneous, but in total neutral clouds of charges, where both molecules are assumed to be in the ground state. By performing multipole expansion of the charge densities the electrostatic energy can further be represented as an interaction energy between dipole-, quadrupole and higher multipole moments. In particular the dipole-dipole contribution relevant for us reads

$$V_{dipole-dipole} = \frac{\mu_1\mu_2}{r_{12}^3}[\hat{\boldsymbol{\mu}}_1 \cdot \hat{\boldsymbol{\mu}}_2 - 3(\hat{\boldsymbol{\mu}}_1 \cdot \hat{\mathbf{r}}_{12})(\hat{\boldsymbol{\mu}}_2 \cdot \hat{\mathbf{r}}_{12})]. \tag{1}$$

- **The induction energy**. It is obtained if one of the two molecules is in an excited state while the other is in the ground state. Such terms describe the distortion of the charge distribution of one molecule by fixed distribution of charges of the other, yielding what is known as dipole-induced dipole, quadrupole and multipole interactions. Again the leading term takes the form

$$V_{dipole-induced\,dipole} = -\frac{V_0\bar{\alpha}\mu^2}{r_{12}^6}\,[\,1 + P_2(\hat{\boldsymbol{\mu}}_1 \cdot \hat{\boldsymbol{a}}_2)P_2(\hat{\boldsymbol{a}}_2 \cdot \hat{\mathbf{r}}_{12}) + P_2(\hat{\boldsymbol{\mu}}_2 \cdot \hat{\boldsymbol{a}}_1)P_2(\hat{\boldsymbol{a}}_1 \cdot \hat{\mathbf{r}}_{12})\,]\,. \tag{2}$$

- **The dispersion energy**. It is obtained if both molecules are in excited states and can be thought of as an interaction between mutually excited charge distributions on both molecules. An example is provided by the standard induced dipole-induced dipole interaction

$$V_{dispersion} = -\frac{1}{r_{12}^6}\{V_1[\hat{\boldsymbol{a}}_1 \cdot \hat{\boldsymbol{a}}_2 - 3(\hat{\boldsymbol{a}}_1 \cdot \hat{\mathbf{r}}_{12})(\hat{\boldsymbol{a}}_2 \cdot \hat{\mathbf{r}}_{12})]^2 + V_2[(\hat{\boldsymbol{a}}_1 \cdot \hat{\mathbf{r}}_{12})^2 + (\hat{\boldsymbol{a}}_2 \cdot \hat{\mathbf{r}}_{12})^2]\}. \tag{3}$$

In the formulas above r_{12} is the distance between the (induced) dipole ($\boldsymbol{a}_1$) $\boldsymbol{\mu}_1$ and the (induced) dipole ($\boldsymbol{a}_2$) $\boldsymbol{\mu}_2$; ($\hat{\boldsymbol{a}}_\alpha$) $\hat{\boldsymbol{\mu}}_\alpha$ is the unit vector parallel to the orientation of the (induced) dipole $'\alpha'$; $\hat{\mathbf{r}}_{12}$ is the unit vector pointing from

the (induced) dipole "1" towards the (induced) dipole "2"; $\bar{\alpha}$ is the average molecular polarizability, and P_2 is the second-order Legendre polynomial.

Defined as above, the dispersive forces are expected to be strongly sensitive to the molecular electron distribution. Since the electron density defines the molecular shape the anisotropy of dispersive forces follows, in most cases, the molecular shape anisotropy. For "sufficiently" anisotropic molecules and for fixed distances between the centers of mass of the molecules the minimum of the dispersive part of the interaction is thus expected for parallel alignment of the long molecular axes.

Two different approaches are now possible. In the first one we may think of the interaction between *total* molecular multipole moments, referred to the center of mass of the molecule. An often used alternative approach divides each of the two molecules into "well localized" electronic units. If the localization of the units can indeed be justified the interaction between the molecules can be viewed as interaction between each of the units. Hence, the molecule can be regarded as having a certain distribution of *localized* multiple moments (*e.g.* dipole moment associated with the cyano end group of cyanobiphenyles) as well as distribution of induction and dispersion contributions.

A few comments seem appropriate at this place:

- In our discussion we have disregarded three-body and, in general, many-body interactions, which may not necessarily be correct for dense systems. However, as far as we are aware of no systematic studies exist to date of many body interactions on liquid crystalline properties.
- There are other contributions to pair interactions not discussed here like resonance and magnetic ones, but they are much weaker as compared to the ones already introduced. We may also think of modifications due to molecular flexibility or specific molecular shape.
- We have so far discussed some general features of pair interactions for anisotropic molecules. The approach as given, although very successful for an identification of relevant terms characterizing potential energy of two molecules, is not easily applicable for quantitative, *ab initio* predictions of liquid crystalline properties. One is often forced to use a series of additional simplifying assumptions thus making the final formulae severely limited.

Owing to the technical difficulties in *ab initio* modelling of real pair interactions between large molecules it is often more appropriate to use an alternative, semi-empirical description. In such approach the actual intermolecular interactions are approximated by functions depending on a number of adjustable parameters which, if necessary, can be fitted to experimental data. One commonly used form is the atom-atom Lennard-Jones interaction with attractive and repulsive parts that decay as 6th and 12th inverse powers of

distance

$$V_{LJ} = \sum_{ab} 4\epsilon_{ab} \left[\left(\frac{\sigma_{ab}}{r_{ab}} \right)^{12} - \left(\frac{\sigma_{ab}}{r_{ab}} \right)^{6} \right], \tag{4}$$

where ϵ_{ab} is the potential well depth, and σ_{ab} is the shape parameter (*i.e.* distance at which the potential changes sign) for the interaction between atoms a on the molecule '1' and atoms b on the molecule '2'. Note that V, Eq.(4), includes part of attractive dispersion forces (3) and approximates repulsion at short distances. Terms that are normally added to (4) involve Coulomb, bond bending and torsional interactions. Detailed examples are discussed by Cook and Wilson in their atomistic simulations of liquid crystalline systems in the isotropic phase [27].

3.2 Gay-Berne pair potential

A difficulty in using realistic potentials like (4) for computer simulations is that they become computationally extremely expensive for large molecules [27]. Alternatives that proved very successful in modelling the general behavior of liquid crystals are single site potentials that depend not only on the relative distance between the centers of mass of the molecules, but also on the mutual molecular orientations. One of the most popular pair interaction belonging to this class is a nonspherical version of the Lennard-Jones potential (4) as introduced by Gay and Berne [28]. For molecules of uniaxial symmetry it depends on the unit vectors $\hat{\mathbf{e}}_i$ and $\hat{\mathbf{e}}_j$ describing the orientations of a pair of molecules and on the separation vector $\mathbf{r} = \mathbf{r}_i - \mathbf{r}_j$ of their centers of mass $\mathbf{r}_i$ and $\mathbf{r}_j$. The detailed expressions are

$$V_{GB}(\hat{\mathbf{e}}_i, \hat{\mathbf{e}}_j, \mathbf{r}) = 4\,\epsilon(\hat{\mathbf{e}}_i, \hat{\mathbf{e}}_j, \hat{\mathbf{r}})\,\left(R^{-12} - R^{-6}\right), \tag{5}$$

where

$$R = \left[r - \sigma(\hat{\mathbf{e}}_i, \hat{\mathbf{e}}_j, \hat{\mathbf{r}}) + \sigma_0 \right] / \sigma_0. \tag{6}$$

Here $r = |\mathbf{r}|$ is the length of the separation vector and $\hat{\mathbf{r}} = \mathbf{r}/r$ is the unit vector describing its orientation.

The Gay-Berne potential (5) is thus an anisotropic and shifted version of the potential (4). It differs from (4) in that both the potential well ϵ and the molecular shape parameter σ [2] are orientationally dependent. Originally the form of ϵ and σ was selected to give the best fit to the pair potential for a linear array of four equidistant point Lennard-Jones particles with a separation of $2\sigma_0$ between the first and fourth sites. The currently used definitions for the well and depth are

$$\sigma(\hat{\mathbf{e}}_i, \hat{\mathbf{e}}_j, \hat{\mathbf{r}}) = \sigma_0 \left\{ 1 - \frac{1}{2}\chi \left[\frac{(\hat{\mathbf{r}} \cdot \hat{\mathbf{e}}_i + \hat{\mathbf{r}} \cdot \hat{\mathbf{e}}_j)^2}{1 + \chi\,(\hat{\mathbf{e}}_i \cdot \hat{\mathbf{e}}_j)} + \frac{(\hat{\mathbf{r}} \cdot \hat{\mathbf{e}}_i - \hat{\mathbf{r}} \cdot \hat{\mathbf{e}}_j)^2}{1 - \chi\,(\hat{\mathbf{e}}_i \cdot \hat{\mathbf{e}}_j)} \right] \right\}^{-1/2} \tag{7}$$

[2] Molecular shape is defined through the equipotential surface $V_{GB} = 0$, for which we have $r|_{V_{GB}=0} = \sigma$

$$\epsilon(\hat{\mathbf{e}}_i, \hat{\mathbf{e}}_j, \hat{\mathbf{r}}) = \epsilon_0\, \epsilon^{\nu}(\hat{\mathbf{e}}_i, \hat{\mathbf{e}}_j)\, \epsilon'^{\mu}(\hat{\mathbf{e}}_i, \hat{\mathbf{e}}_j, \hat{\mathbf{r}}) \tag{8}$$

and

$$\epsilon(\hat{\mathbf{e}}_i, \hat{\mathbf{e}}_j) = \left[1 - \chi^2\, (\hat{\mathbf{e}}_i \cdot \hat{\mathbf{e}}_j)^2\right]^{-1/2} \tag{9}$$

$$\epsilon'(\hat{\mathbf{e}}_i, \hat{\mathbf{e}}_j, \hat{\mathbf{r}}) = 1 - \frac{1}{2}\,\chi' \left[\frac{(\hat{\mathbf{r}} \cdot \hat{\mathbf{e}}_i + \hat{\mathbf{r}} \cdot \hat{\mathbf{e}}_j)^2}{1 + \chi'\, (\hat{\mathbf{e}}_i \cdot \hat{\mathbf{e}}_j)} + \frac{(\hat{\mathbf{r}} \cdot \hat{\mathbf{e}}_i - \hat{\mathbf{r}} \cdot \hat{\mathbf{e}}_j)^2}{1 - \chi'\, (\hat{\mathbf{e}}_i \cdot \hat{\mathbf{e}}_j)} \right]. \tag{10}$$

The potential contains six parameters $(\kappa, \kappa', \mu, \nu)$ and (σ_0, ϵ_0). The first four determine the anisotropy of the repulsive and attractive forces while the other two introduce a natural length and energy scale. The parameters χ and χ' in (7-10) are related to the length-to-breadth ratio κ and potential well depths ratio κ' for the side-to-side and end-to-end molecular configurations

$$\chi = \frac{\kappa^2 - 1}{\kappa^2 + 1}\,, \tag{11a}$$

$$\chi' = \frac{\kappa'^{1/\mu} - 1}{\kappa'^{1/\mu} + 1}. \tag{11b}$$

They both vanish for spherical particles while χ is $+1$ for infinitely long rods and -1 for infinitely thin disks. The pair (σ_0, ϵ_0) corresponds to the shape parameter and well depth calculated for a configuration when all three molecular vectors $\hat{\mathbf{e}}_i$, $\hat{\mathbf{e}}_j$, and $\hat{\mathbf{r}}$ are mutually perpendicular (cross configuration). The last two parameters, μ and ν, tune the shape of the well depth in a more subtle way. In particular, the role of μ is comprehended, to a large extend, by relation (11b) while ν is connected to the well depth ratio κ'' for the side-to-side and cross configurations

$$\kappa'' = \frac{1}{(1 - \chi^2)^{\nu/2}}. \tag{12}$$

As already indicated before the parameters ϵ_0 and σ_0 of the Gay-Berne potential provide a natural length and energy scale. In terms of these constants all relevant physical quantities can be rendered dimensionless. The most often used (dimensionless) reduced quantities (denoted by a star) are listed below:

- length: $l^* = l/\sigma_0$
- time: $t^* = \sqrt{m\sigma_0^2/\epsilon_0}$
- density: $\rho^* = \rho\, \sigma_0^3$
- energy: $E^* = E/\epsilon_0$
- temperature: $T^* = kT/\epsilon_0$
- dipole moment: $\mu^* = \mu\, (\epsilon_0 \sigma_0^3)^{-1/2}$.

Among the cases studied the original Gay-Berne model (OGB) [28], defined by $\kappa = 3$, $\kappa' = 5$, $\mu = 2$ and $\nu = 1$, is the one most thoroughly

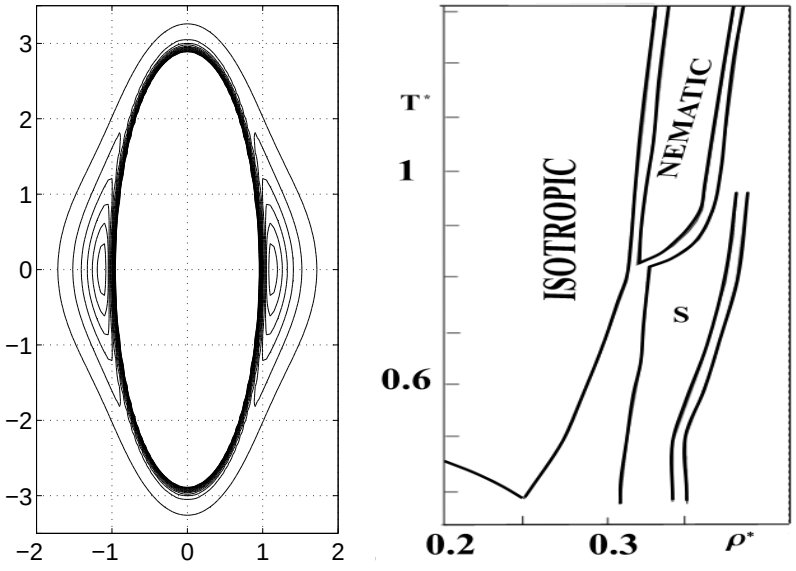

(**a**) (**b**)

Fig. 5. (**a**)The potential energy contours calculated for a pair of Gay-Berne particles. The molecules are assumed to be parallel to the z axis of the laboratory frame. The center of the reference molecule is located at the origin of laboratory frame. Owing to the cylindrical symmetry of the interactions only $x-z$ cross section of the potential is shown. The contours are parameterized by the dimensionless potential energy (V_{GB}/ϵ_0). The innermost contours correspond to 2 and the other contours are for values of the scaled potential energy decreasing in steps of 0.25 until -5. In this figure and in all figures that follow quantities are given in reduced units. (**b**) Schematic representation of the corresponding phase diagram as determined from simulations by Miguel *et al.* [31]

documented in the literature [29–31]. Its potential energy contours for the long molecular axes parallel to each other are shown in Fig.(5a).

Clearly, the OGB potential prefers a side-to-side arrangement of the pair of molecules which, in turn, promotes liquid crystallinity. The length-to-breadth ratio[3] is 3:1, as the value of κ suggests, and this seems to be the minimum value that is found experimentally for molecules forming liquid crystals. The complete phase diagram for this model is found in [31] and its sketch is shown in Fig.(5b). It is particularly simple, revealing only vapor, isotropic liquid, nematic and smectic B phases.

The Gay-Berne potential is very rich in predictions and remarkably successful in computer simulations of liquid crystalline phases. Using molecular

[3] It is defined as a ratio of distances corresponding to $V_{GB} = 0$ for end-to-end and side-to-side configurations

dynamics and Monte Carlo techniques a phase behavior of the four-parameter Gay-Berne potential has been studied to prove that the model agrees well with what is observed for real mesogens [29–33].

In view of this success the original Gay-Berne potential has been developed further to include molecular biaxiality [34] (and to stabilize biaxial nematic phase [35]), flexibility [36], more complex molecules composed of a collection of Gay-Berne sites [37], dipolar forces [38–49], steric dipoles [18] and *zig-zag* shaped molecules [50].

Extension of the Gay-Berne potential to include dipole-dipole interactions due to a permanent dipole moment is straightforward. In this case the pair potential energy (5) should be supplemented by the contribution (1)

$$V = V_{GB} + V_{dipole-dipole}. \tag{13}$$

Just to have an impression what the potential energy for a pair of dipolar Gay-Berne particles looks like we sketch the energy contours in Fig.(6) for the OGB potential with a single longitudinal dipole moment per molecule. Note changes of the contours on going from central to terminal dipoles.

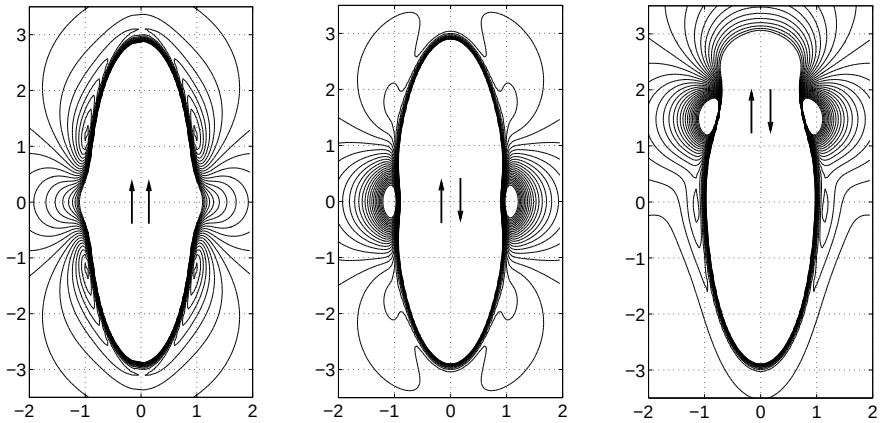

Fig. 6. The potential energy contours calculated for a pair of Gay-Berne particles with embedded longitudinal dipole moment. The molecules and the dipole moments are taken parallel to the z axis of the laboratory frame. The center of the reference molecule is located at the origin of the laboratory frame. The contours are parameterized by the dimensionless total potential energy (V/ϵ_0). The innermost contours correspond to 2 and the other contours are for values of the scaled potential energy decreasing in steps of 0.25 until -5. Orientation and localization of the dipole moments along the molecules is indicated by arrows. The position $d^* = 2 \times$ *(actual position from molecular center)*$/\sigma_0$ of the dipoles is: (**a**) d^* arbitrary, (**b**) $d^* = 0$, (**c**) $d^* = 0.75$. In all cases the value of the dipole moment is $\mu^* = 2.5$

As the OGB with longitudinal dipole moments is one of the most frequently studied polar version of the Gay-Berne potential we are going to discuss in detail the relation between the strength and position of the longitudinal dipole moment on the formation of mesophases. Not only central and terminal, but also intermediate positions of the dipoles are considered. The discussion will be illustrated with the results obtained for an ideally oriented polar version of the OGB system with longitudinal dipoles [48], here referred to as IOGB. In the IOGB model the translational degrees of freedom of the molecules are unrestricted but their orientations are fixed parallel to the z axis of the laboratory frame. That is the dipoles can be oriented either parallel or antiparallel to the positive z axis and are given by $\boldsymbol{\mu}_i = \mu\, s_i \hat{\mathbf{z}}$, where $s_i = \pm 1$. Their location on the molecular axis is given by a parameter d^* (*see* Fig.(6)), which denotes the distance of the dipole from the molecular center.

At high temperatures, the IOGB model exhibits an ideally oriented nematic phase, which is the reference state of the system. In the limit of vanishing dipole moment nematic[4], smectic A and smectic B phases are stable. The simplification of the ideal nematic order is reasonable whenever structures with strong alignment are expected, which is the case for smectic- and crystalline phases of the polar OGB system.

4 Computer simulations with dipoles

Simulations of a system can be done at many different levels of fidelity. The simulations dealt with here are Molecular Dynamics (MD) and Monte Carlo (MC) simulations for a classical system of molecules interacting through a potential like (13). Our goal is to extract information about equilibrium bulk properties for given temperature and pressure (or density). We do not intend to discuss here specific MD or MC algorithms used in simulations, which are well presented in [15,16], but rather describe essential details specific to the analysis of phase behavior of polar mesogens.

Usually a simulation for a system with dipoles is carried out for an ensemble of a few hundred to a few thousand of molecules. Though the number depends strongly on actual computational resources available and on the problem studied a system size dependence was observed when the number of particles was less than 500 (*see e.g.* simulation for dipolar hard-core system [53]). This dependence may result from a combination of the long-range nature of dipolar (or generally electrostatic) interactions, approximations used to calculate them and the structure analyzed. Importantly, the system size sets up the limit for the allowed wavelengths of fluctuations. Hence the correlation length in the system that we simulate should actually be smaller than the system size. In studying systems close to a second- or weakly first order phase transition, where usually the correlation length exceeds the system

[4] Nematic phase of perfectly oriented Gay-Berne model without dipoles has been studied by Wagner [51,52]

size, a finite size scaling analysis of quantities looked for is necessary. As a rule, it is always important to carry out tests with larger systems for possible finite size effects, especially for systems with long-range interactions.

Assume now that our collection of molecules is restricted to a rectangular volume $L_x \times L_y \times L_z$. With a small system size we cannot simulate correctly bulk properties as a considerable number of particles resides on its surface (about 49% for a cubic box of 1000 molecules). To overcome this difficulty one usually introduces periodic boundary conditions where the system of interest, called central box, is surrounded by identical systems *i.e.* with exactly the same configuration of molecules at any moment of simulations [15]. As a particle moves through a boundary its image from a neighboring box enters and hence the constant density is maintained in every box as well as in the whole system. It is assumed that the behavior of a real, infinite system is most similar to that composed of periodic images of the central box. The interaction potential of the real system can now be approximated by an interaction between any two particles i and j of the central box and their images. It is thus given by the following expression

$$V = \frac{1}{2} \sum_{i \neq j} V_{PBC}(\mathbf{r}_i, \mathbf{r}_j, \ldots) + \sum_i V_{PBC}(\mathbf{r}_i, \mathbf{r}_i, \ldots) \tag{14}$$

where

$$V_{PBC}(\mathbf{r}_i, \mathbf{r}_j, \ldots) = \sum_{\mathbf{m}}{}' V(\mathbf{r}_i - \mathbf{r}_j + \sum_{\alpha=x,y,z} \mathbf{L}_\alpha \, m_\alpha, \ldots). \tag{15}$$

The sum in Eq.(15) runs over all vectors $\mathbf{m}$ with integer coefficients m_α, and $\mathbf{L}_\alpha$ are the vectors of length L_α parallel to the edges of the box. The prime indicates that for $\mathbf{m} = \mathbf{0}$ the terms with $i = j$ are to be omitted. Note that $\mathbf{r}_j - \sum_{\alpha=x,y,z} \mathbf{L}_\alpha m_\alpha$ are image particles of the particle $'j\,'$ and that the second term in Eq.(14) represents interaction of the particle $'i\,'$ with all its images. Clearly, only positions and orientations of the molecules in the central box are to be stored during simulations.

Usually special techniques, discussed in the next subsections, are needed to have a credible estimate of the infinite sum (14) for the electrostatic part of the interactions. The trouble, in particular with the dipole-dipole interaction, is due to its long range. The sum (14) is only conditionally convergent in this case, which means that the result depends on the way in which we add up the terms. It also means that the straight truncation of the dipole-dipole interaction at a given (spherical) cutoff (so that the interactions beyond cutoff are neglected) is generally not acceptable at the cutoff distances commonly used for simulations[5]. Such straight truncation is known to yield wrong predictions for energetic, dynamical and dielectric properties of the system. We

[5] A standard potential cutoff, which we utilize for the Gay-Bernie part of (15) is $r^*_{cut} = 4.0$, *i.e.* $V_{GB} = 0$ for $r > r_{cut}$. Correspondingly, the system size $L_{min} = \min(L_x, L_y, L_z)$ must be taken greater than $2\,r_{cut}$. Choosing L_{min} we must be

should add that the proper treatment of the dipolar forces is the most time consuming part of the simulations and it is this part of the code that limits the system size in practice.

The available methods fall into two categories, the explicit molecule-molecule description and the molecule-continuum description. Two most commonly used representatives of these methods are the Ewald summation technique [15,16,54–64] and the Onsager reaction-field [15,62–66] method, respectively. The Ewald summation technique treats essentially in an exact manner the interaction between the dipoles in the central box and its periodic replicas, whereas the Onsager reaction field replaces "uninteresting" dipole moments, located beyond the cutoff radius from a given dipole, by a dielectric continuum. Recently, some improvements over the original techniques also have been proposed [67–70].

4.1 Ewald summation technique for dipolar interactions

The Ewald summation technique for the calculation of the dipole-dipole part in the sum (15) is probably the most reliable one available today. It could be introduced using a few equivalent formulations but from a mathematical point of view it amounts in multiplying each m-dependent term in (15) by a convergence factor, usually of the Gaussian form $\exp(-s|\mathbf{m}|^2)$, which makes (15) absolutely convergent. If we then calculate the so modified lattice sum by any correct method and take the limit of $s \to 0$ afterwards, we obtain a finite result. It becomes equivalent to performing a conditional summation (15) over spherical shells. The dipole-dipole part of the potential energy (14) so calculated splits itself into rapidly converging real- and Fourier-space lattice sums. More specifically, it is being reduced to four different terms: *(a)* a real term arising from the short-range interaction in the real space; *(b)* a reciprocal term arising from the long-range interaction in the reciprocal space; *(c)* a self-energy term correcting the contribution in the reciprocal space, and *(d)* a surface term connected with the continuum surrounding the replicated sample. They read [64,71]

$$\begin{aligned} V_{dd} = \frac{1}{2} \sum_{i \neq j} (\boldsymbol{\mu}_i \cdot \boldsymbol{\mu}_j)\, B(r_{ij}) - (\boldsymbol{\mu}_i \cdot \mathbf{r}_{ij})\, (\boldsymbol{\mu}_j \cdot \mathbf{r}_{ij})\, C(r_{ij}) \\ + \frac{2\pi}{V} \sum_{\mathbf{k} \neq 0} \frac{\exp(-k^2/4\gamma^2)}{k^2} |F(\mathbf{k})|^2 - \frac{2\gamma^3}{3\sqrt{\pi}} \sum_{i=1}^{N} \boldsymbol{\mu}_i^2 \\ + \frac{2\pi}{(2\epsilon_{surr} + 1)\, V} \left(\sum_{i=1} \boldsymbol{\mu}_i \right)^2 . \end{aligned} \tag{16}$$

---

aware of finite size effects when the actual correlation length in the system is comparable with L_{min}

In the expression above $\mathbf{k}$ denotes the reciprocal lattice vector given by $\mathbf{k} = (2\pi n_x/L_x,\ 2\pi n_y/L_y,\ 2\pi n_z/L_z)$ with $n_x,\ n_y,\ n_z = 0, .., n_{\max}$ and γ is the convergence parameter. The functions $B(r_{ij})$ and $C(r_{ij})$ are defined as

$$B(r_{ij}) = \frac{\mathrm{erfc}(\gamma r_{ij})}{r_{ij}^3} + 2\,\frac{\gamma}{\sqrt{\pi}}\,\frac{\exp(-\gamma^2\, r_{ij}^2)}{r_{ij}^2} \tag{17}$$

and

$$C(r_{ij}) = 3\,\frac{\mathrm{erfc}(\gamma r_{ij})}{r_{ij}^5} + 2\,\frac{\gamma}{\sqrt{\pi}}\left(2\gamma^2 + \frac{3}{r_{ij}^2}\right)\frac{\exp(-\gamma^2\, r_{ij}^2)}{r_{ij}^2}, \tag{18}$$

whereas the so-called dipole structure factor $|F(\mathbf{k})|^2$ is given by

$$F(\mathbf{k}) = \sum_{i=1}^{N} (\boldsymbol{\mu}_i \cdot \mathbf{k})\, \exp(\mathrm{i}\,\mathbf{k}\cdot\mathbf{r}_i); \tag{19}$$

$\mathrm{erfc}(x) = \frac{2}{\sqrt{\pi}} \int_x^\infty \mathrm{d}t\, e^{-t^2}$ is the complementary error function. Finally, the surface term acts as a depolarization field and is due to the total dipole moment of the central box confined in the volume V. The parameter ϵ_{surr} that enters the surface term is the dielectric constant of the continuum surrounding the whole system *i.e.* central box plus all its replicas. Actually it is not clear what is the best choice for ϵ_{surr}. Assuming that the surrounding medium is the same as the bulk one this parameter should be found selfconsistently so that the bulk dielectric constant is equal to the surface one. However, this would considerably slow down simulation so the standard choice for ϵ_{surr} is an *a priori* value taken to be either infinity (tinfoil or metal boundary conditions) or 1 (vacuum boundary conditions). For dipolar systems the first extreme value would be most desirable because it makes the surface term vanish. Indeed when the net polarization in the simulation cell could be disregarded ($\sum_{i=1}^{N} \boldsymbol{\mu}_i/N \approx 0$), as *e.g.* for structures with no net polarization, adopting tinfoil boundaries seems legitimate[6] as there is no considerable polarization effects coming from the bulk. But this term is not necessarily negligible when there is a net dipole moment in the simulation cell and it may modify the internal energy in an essential way. Thus, in general, the choice of the boundary conditions may have an influence on the results of simulations [71–73].

The infinite Ewald sum, Eq.(16), is independent of the convergence parameter γ. In the calculations, however, when only a finite number of terms can be considered, γ and the number of $\mathbf{k}$ vectors are adjustable parameters and are typically chosen to optimize computations. In particular γ is usually chosen large so that the sum in real space disregards pairs separated more

[6] Exception here could be a calculation of the dielectric constant, which may depend on the boundaries adopted

than $L_{min}/2$, where $L_{min} = \min(L_x, L_y, L_z)$. Typically, one uses $\gamma \cong 5/L_{min}$ and includes about 100-500 wavevectors in the sum over reciprocal space. An analysis of the errors resulting from such truncation of both series has been reported by Neumann *et al.* [58], Kolafa *et al.* [59], Fincham [60] and Hummer [61]. In particular Hummer [61] has proposed an empirical rule allowing to achieve the same accuracy for the Fourier sum with two different values of γ. The rule states that the corresponding **k**-space cutoff distances have to be chosen according to $|\mathbf{n}_{1,max}|/|\mathbf{n}_{2,max}| = \gamma_1/\gamma_2$.

In our simulations of the IOGB systems [48] at densities of the order of 0.3 we found that the optimal value for the parameter γ is $5.75/L_{min}$. With this choice of γ the real space part of the Ewald sum could indeed be limited to the central box and the Fourier space part restricted to vectors $\mathbf{k} = (2\pi n_x/L_x,\, 2\pi n_y/L_y,\, 2\pi n_z/L_z)$, such that $|\mathbf{n}| = \sqrt{n_x^2 + n_y^2 + n_z^2} \leq 6$.

4.2 Reaction field method

A direct use of the Ewald summation technique is computationally very expensive, especially for large systems. Another widely used approach, which stays relatively cheap, is the Onsager reaction field method [65,66]. In this method each particle "i" interacts with other particles confined within a sphere S_i of radius r^*_{cut}. The medium outside the cutoff sphere of each molecule is replaced by a uniform dielectric continuum with a static dielectric constant ϵ_{RF}. It gives rise to a reaction field $\mathbf{E}_{RF,i}$ on the dipole "i". The solution of the Maxwell equations adequate to the above approximation yields an electric field at the center of the sphere given by

$$\mathbf{E}_{RF,i} = \frac{2(\epsilon_{RF} - 1)}{(2\epsilon_{RF} + 1) r^3_{cut}} \mathbf{M}_i, \tag{20}$$

where $\mathbf{M}_i$ is the total dipole moment of the sphere S_i. A dipole $\boldsymbol{\mu}_i$ immersed in the field (20) has a potential energy

$$V_{RF,i} = -\frac{2(\epsilon_{RF} - 1)}{(2\epsilon_{RF} + 1)} \frac{\mathbf{M}_i \cdot \boldsymbol{\mu}_i}{r^3_{cut}}. \tag{21}$$

Consequently, the dipole-dipole energy of the whole system is

$$V_{dd} = \frac{1}{2} \sum_{i \neq j} \left[V_{dipole-dipole}(\mathbf{r}_{ij}) - \frac{2(\epsilon_{RF} - 1)}{(2\epsilon_{RF} + 1)} \frac{\boldsymbol{\mu}_i \cdot \boldsymbol{\mu}_j}{r^3_{cut}} \right] \theta(r_{cut} - r_{ij}), \tag{22}$$

where θ is the theta Heaviside function. As expected, the reaction field vanishes for vacuum ($\epsilon_{RF} = 1$) whereas it is maximal for metallic ($\epsilon_{RF} = \infty$) surroundings. Its action on the system is to polarize molecules in the central box. Hence the direct antiferroelectric ordering between the dipole moments is weakened. As ϵ_{surr} for the Ewald method the true ϵ_{RF} should be calculated selfconsistently so that the average dielectric constant of the central

box agrees with ϵ_{RF}. But in practice, as in the case of the Ewald summation, the simulations are often carried out with a fixed value of $\epsilon_{RF} >> 1$. For example, in the case of the structures with vanishing *average* dipole moment of the central box, a substitution $\epsilon_{RF} = \infty$ is usually a satisfactory choice. The detailed value of ϵ_{RF}, given it is large, does not affect significantly calculated thermodynamic properties and correlation functions in this case. This has been explicitly demonstrated for the Stockmayer fluid [74] in liquid and vapor phases, and for the dipolar Gay-Berne with longitudinal dipole moments where both selfconsistent and tin-foil values of ϵ_{RF} have been used [48,49,62,63].

To complete this subsection we note that the Ewald summation and the approximate reaction field method are not equivalent. This is quite clear if we compare the respective formulas (16) and (22). While the Ewald technique correctly accounts for long-range nature of the dipolar forces the reaction field method turns the dipole-dipole interaction into a spherically symmetric, relatively short-ranged effective potential, like the Gay-Berne one [7]. However, for many cases studied in the literature concerned with polar Gay-Berne systems [48,49,62–64] the differences between the use of the Ewald summation and the reaction field with conducting boundary conditions ($\epsilon_{RF} = \infty$) appear to be of secondary importance. This holds true both for nonpolar liquid phases like nematic and isotropic liquids and for nonpolar crystalline phases. The proper use of the reaction field requires, however, the use of a selfconsistently calculated averaged dielectric constant ϵ_{RF}.

4.3 Further computational details

Simulations of model polar liquid crystalline systems can be carried out using either classical Molecular Dynamics (MD) or Monte Carlo (MC) methods. They allow to find a direct connection between pair interactions and the corresponding structural, dynamic and energetic properties of the system. Simulations are usually performed in the NVT (constant number of molecules N, volume V and temperature T) or NPT (constant number of molecules N, pressure P and temperature T) ensemble as described in [15,16]. In order to investigate the phase behavior of mesogenic systems constant pressure simulations (NPT) seem more suitable, especially for small systems. By allowing the central box dimensions to change the natural smectic and crystal structures can easily fit the dimensions of the simulation box, which is harder to achieve in the NVT ensemble.

But when dipolar interactions are calculated using the Ewald summation technique, the NPT simulations are computationally much more expensive than the NVT simulations. The reason is the necessity of recalculating tabulated earlier wave vectors and consequently also wave vector dependent terms $\exp(-k^2/4\gamma^2)/k^2$ in Eq.(16) when the box dimensions are changed.

[7] A generalization of the reaction field to include a possible anisotropy of the dielectric continuum also is possible although we are not aware of such analysis

A typical time step taken in MD simulations for the integration of the equations of motion is $\delta t^* \simeq 0.001 t^*$. Usually about $10^4 - 10^6$ timesteps are needed to equilibrate the system of more than 500 molecules. Quantities of interest are calculated and averaged over $10^4 - 10^6$ additional timesteps. Large runs are needed especially close to a phase transition.

A single time step in a MD run corresponds to one cycle of MC simulation, where one cycle represents N trial displacements and reorientations of the molecules at constant volume followed by one attempted box length move. The last step applies, of course, only when NPT simulations are carried out. The parameters controlling maximal increment of the displacements, the orientations and of the box dimensions are chosen such that the acceptance ratio for attempted moves is between 20% and 50%.

5 Structure analysis

The structures of liquid crystalline phases identified in simulations are characterized in terms of the probability densities for finding groups of one, two, or more molecules at specified positions and orientations in phase space [76–78]. The most important of these are the singlet and the pair distributions. They can be used to calculate some of the equilibrium properties of mesophases, like the total average potential energy, pressure, specific heat, *etc.* [76–78].

In this section we are going to discuss in detail various singlet, pair and three-body distribution functions and the way in which they can be extracted from the simulation data. We demonstrate, by referring to an ideally oriented system of Gay-Berne molecules with embedded longitudinal dipole moments [48], that all these functions are necessary to elucidate the short-range and long-range organization in liquid crystalline phases formed by polar systems. In particular, the importance of triplet correlations for a proper understanding of the structures and of their local, dipolar organization is demonstrated. In order to simplify the notation we assume that the model mesogenic molecules are axially symmetric with inversion symmetry, *i.e.* only longitudinal components of the dipole moments are considered. Generalization to the biaxial case, as induced *e.g.* by transversal dipoles, is straightforward [76].

5.1 Singlet distribution functions and order parameters

The simplest of the distribution functions is the one-particle density distribution function. For liquid crystals composed of uniaxial molecules it is defined as

$$P^{(1)}(\mathbf{r}, \hat{\mathbf{\Omega}}) = \frac{1}{N} < \sum_{i=1}^{N} \delta(\mathbf{r} - \mathbf{r}_i{}') \, \delta(\hat{\mathbf{\Omega}} - \hat{\mathbf{\Omega}}_i{}') >, \tag{23}$$

where δ is the Dirac delta function and the ensemble average $< ... >$ is performed over primed variables representing the molecular positions and orientations. Clearly, $P^{(1)}(\mathbf{r},\hat{\mathbf{\Omega}})\,\mathrm{d}^3\mathbf{r}\,\mathrm{d}\hat{\mathbf{\Omega}}$ gives the probability of finding a mesogenic molecule within the range $[\,\mathbf{r},\mathbf{r}+\mathrm{d}\mathbf{r}\,]$ of positions and the range $[\,\hat{\mathbf{\Omega}},\hat{\mathbf{\Omega}}+\mathrm{d}\hat{\mathbf{\Omega}}\,]$ of orientations, where the latter being represented by the unit vector $\hat{\mathbf{\Omega}}$. Integration of $P^{(1)}$ over positions and orientations yields the normalization condition: $\int \mathrm{d}^3\mathbf{r}\,\mathrm{d}\hat{\mathbf{\Omega}}\; P^{(1)}(\mathbf{r},\hat{\mathbf{\Omega}}) = 1$.

Associated with the distribution function (23) are the order parameters. They can be introduced by referring to the Fourier integral representation of the spatial Dirac delta function: $\delta(\mathbf{r}) = \frac{1}{V}\sum_{\mathbf{k}} e^{i\,\mathbf{k}\cdot\mathbf{r}}$ and the representation of the angular delta: $\delta(\hat{\mathbf{\Omega}}-\hat{\mathbf{\Omega}}\,') = \sum_{L,m} Y_m^L(\hat{\mathbf{\Omega}})\,Y_m^L(\hat{\mathbf{\Omega}}\,')^*$, where $k_i = \frac{2\pi m_i}{L_i}$; $m_i = 0,\pm1,...$; $i = x,y,z$, and where the functions Y_m^L are the spherical harmonics [79]. Substitution of these representations into (23) yields

$$P^{(1)}(\mathbf{r},\hat{\mathbf{\Omega}}) = \frac{1}{V}\sum_{\mathbf{k},L,m} P_{\mathbf{k}Lm}\, e^{i\,\mathbf{k}\cdot\mathbf{r}}\; Y_m^L(\hat{\mathbf{\Omega}})\;, \tag{24a}$$

$$P_{\mathbf{k}Lm} = \frac{1}{N} < \sum_{i=1}^{N} e^{-i\,\mathbf{k}\cdot\mathbf{r_i}\,'}\; Y_m^L(\hat{\mathbf{\Omega}}_\mathbf{i}\,')^* > . \tag{24b}$$

The averages $P_{\mathbf{k}Lm}$ are just the order parameters and many of them vanish in practice. In general, the set of indices $\{\,\mathbf{k},L,m\}$ giving nonzero values for $P_{\mathbf{k}Lm}$ can be selected by referring to irreducible representations of the space group associated with the structure. Identification of nonzero $\{\,\mathbf{k},L,m\}$ is particularly simple for uniaxial nematics and for orthogonal uniaxial smectics with one dimensional density modulation [76,81]. In the former case there is no dependence on positions in Eq.(24a), due to the translational symmetry of the nematics. That is, only $P_{\mathbf{0}Lm} =< P_L > Y_m^L(\hat{\mathbf{n}})^*$ order parameters, with $< P_L >$ being the average value of the L-th order Legendre polynomial, are nonzero [79]. It yields

$$\begin{aligned} P^{(1)}(\mathbf{r},\hat{\mathbf{\Omega}}) = P^{(1)}(\hat{\mathbf{\Omega}}) &= \frac{1}{V}\sum_{L} < P_L > \sum_{m=-L}^{L} Y_m^L(\hat{\mathbf{\Omega}})\,Y_m^L(\hat{\mathbf{n}})^* \\ &= \frac{1}{V}\sum_{L}\frac{2L+1}{4\pi} < P_L > P_L(\hat{\mathbf{\Omega}}\cdot\hat{\mathbf{n}}) = P^{(1)}(\hat{\mathbf{\Omega}}\cdot\hat{\mathbf{n}}). \end{aligned} \tag{25}$$

The director dependence of $P_{\mathbf{0}Lm}$ follows from the fact that in the nematic state the global $O(3)$ symmetry is broken to its uniaxial subgroup. In simulations $\hat{\mathbf{n}}$ could be identified with the direction maximizing the expression $< P_L >= \underset{\hat{\mathbf{n}}:|\hat{\mathbf{n}}|=1}{\mathrm{Max}} \frac{1}{N} < \sum_{i=1}^{N} P_L(\hat{\mathbf{\Omega}}_i\,'\cdot\hat{\mathbf{n}}) >$ or, equivalently, with an eigenvector of the alignment tensor [80] $\mathbf{Q} = \frac{1}{2N}\left\langle \sum_{i=1}^{N}(\,3\,\hat{\mathbf{\Omega}}_\mathbf{i}\,'\otimes\hat{\mathbf{\Omega}}_\mathbf{i}\,' - 1)\right\rangle$, corresponding to a nondegenerate eigenvalue.

For nonpolar nematics the states $\hat{\mathbf{n}}$ and $-\hat{\mathbf{n}}$ of the director are equivalent and only terms with even Ls are nonzero in Eq.(25). For polar nematics

[17,18] both even and odd Ls must be retained. In particular, $< P_1 >$ is the average polarization of the phase. Typical forms of the one-particle distribution function (25) for a nematic phase formed in Gay-Berne system along with some values of $< P_2 >$ and $< P_4 >$ are given by Bates and Luckhurst [32].

Our exemplary simulations of polar liquid crystals are restricted to the IOGB model, where $< P_{2L} >= 1$. In this case the general formulas (23,24a) become much simpler, especially for orthogonal smectics. More specifically, for smectic ordering along the director the one-particle distribution function reduces to $P^{(1)}(s,z)$ given by [48]

$$\begin{aligned} P^{(1)}(s,z) &= \frac{1}{N}\left\langle \sum_{i=1}^{N} \delta_{s,s_i'}\,\delta(z-z_i') \right\rangle \\ &= \frac{1}{2L_z}\left[1 + 2\sum_{n=0} \zeta_{2n+1}\, s\, \cos\left[(2n+1)qz\right] + 2\sum_{n=1} \tau_{2n}\, \cos\left(2nqz\right)\right], \end{aligned} \tag{26}$$

where we introduced smectic (τ_{2n}) and dipolar (ζ_{2n+1}) order parameters. Their definitions follow from the Fourier expansion of $P(s,z)$ under normalization condition: $\sum_{s=\pm 1}\int_0^{L_z} \mathrm{d}z P^{(1)}(s,z) = 1$, with $q = \frac{\pi}{l}$ being the wavelength of the smectic structure and l being the layer spacing. The leading amplitudes ζ_1 and τ_2 are given by

$$\zeta_1 = \underset{\{l\}}{\mathrm{Max}} \left| \frac{1}{N}\left\langle \sum_{j=1}^{N} s_j'\, \exp\left(i\,\pi z_j'/\,l\right) \right\rangle \right| \tag{27}$$

$$\tau_2 = \underset{\{l\}}{\mathrm{Max}} \left| \frac{1}{N}\left\langle \sum_{j=1}^{N} \exp\left(2\,i\,\pi z_j'/\,l\right) \right\rangle \right|. \tag{28}$$

The same procedure can be used to find higher order amplitudes of the singlet distribution function (26).

5.2 Pair distribution functions

The one-particle properties of uniaxial nematics and smectics are well understood. But a similar analysis for pair and higher order distribution functions is still far from being complete. A reason for that becomes clear if we write the definition of the simplest of these functions, namely that of the pair distribution [76,77]

$$\begin{aligned} &P^{(2)}(\mathbf{r}_1, \hat{\mathbf{\Omega}}_1, \mathbf{r}_2, \hat{\mathbf{\Omega}}_2) = \\ &< \sum_{i,j,i\neq j}^{N} \delta(\mathbf{r}_1 - \mathbf{r}_i')\,\delta(\,\hat{\mathbf{\Omega}}_1 - \hat{\mathbf{\Omega}}_i'\,)\,\delta(\mathbf{r}_2 - \mathbf{r}_j')\,\delta(\hat{\mathbf{\Omega}}_2 - \hat{\mathbf{\Omega}}_j') > . \end{aligned} \tag{29}$$

Though (29) seems a straightforward generalization of the formula (23), in practice it appears to be a complex quantity, both to calculate and to represent graphically. Even for uniaxial nematics composed of uniaxial, rigid molecules we need to analyze a function depending on seven variables. Only recently this issue has been resolved by studying a complete set of rotational invariants [82]. Interestingly, it has been shown that the seemingly large group of these invariants can be divided into classes having the same asymptotic behavior at large distances and at high orientational order.

The analysis of pair correlations becomes much easier for the ideal nematic order as present in the IOGB model. In this case a simpler version of $P^{(2)}$ can be introduced through the relation [48]

$$P^{(2)} \equiv P^{(2)}(\mathbf{r}, s_1\hat{\mathbf{z}}, s_2\hat{\mathbf{z}}) = \frac{V}{N^2}\left\langle \sum_i \sum_{j\neq i} \delta_{s_1 s_i}\delta_{s_2 s_j}\delta(\mathbf{r}-\mathbf{r}_i+\mathbf{r}_j)\right\rangle$$
$$= P^{(2)}(r, \hat{\mathbf{r}}\cdot\hat{\mathbf{z}}, s_1 s_2) = \sum_L \frac{2L+1}{2} P_L^{(2)}(r, s_1 s_2)\, P_L(\cos\theta), \tag{30}$$

where θ is the angle between the unit intermolecular vector and $\hat{\mathbf{z}}$. $P^{(2)}$ gives the probability that one particle with dipole orientation s_1 is separated by a distance $\mathbf{r}$ from another with dipole s_2 (irrespective of their absolute positions), relative to the probability expected for a completely random distribution at the same density. It represents pair correlations of translationally invariant phases and is an approximation of the correlations for crystalline structures.

There are two pair distribution functions that can be derived from $P^{(2)}$, which are of particular interest for layered structures. One is the axial pair distribution function, $P_\parallel^{(2)}(z, s_1 s_2)$, defined as

$$P_\parallel^{(2)}(z, s_1 s_2) = \frac{L_z}{2N^2}\left\langle \sum_i \sum_{j\neq i} \delta_{s_1 s_i}\,\delta_{s_2 s_j}\,\delta(z-|z_i-z_j|)\right\rangle. \tag{31}$$

It gives the probability of finding centers of mass of two particles at a resolved, relative distance of z along the director, and with orientations s_1, s_2 of the molecular dipoles relative to the same probability calculated for an ideal gas of particles at the same density. We calculate $P_\parallel^{(2)}(z, \uparrow\uparrow)$ for pairs of molecules with the same dipolar orientations and $P_\parallel^{(2)}(z, \uparrow\downarrow)$ for pairs of molecules with their dipoles oriented in opposite directions, where $s = 1 \equiv\uparrow$ and $s = -1 \equiv\downarrow$. From these two functions we then obtain $P_\parallel^{(2)}(z)$ for arbitrary orientation of the dipoles by summing over s_1 and s_2.

The structure perpendicular to the director can be probed with the transversal pair distribution function, $P_\perp^{(2)}(r_\perp, s_1 s_2)$, where $r_\perp$ is the distance between the centers of mass of particles projected onto a plane orthogonal to

$\hat{\mathbf{z}}$. It is defined by [48]

$$P_{\perp}^{(2)}(r_{\perp}, s_1 s_2) = \frac{1}{4\pi D} \int_0^{2\pi} \mathrm{d}\phi \int_{-D}^{D} \mathrm{d}z \; P^{(2)}(r_{\perp}, \phi, z, s_1 s_2) = \frac{V}{4\pi r_{\perp} D N^2}$$
$$\times \left\langle \sum_i \sum_{j \neq i} \delta_{s_1 s_i} \, \delta_{s_2 s_j} \, \delta(r_{\perp} - |\mathbf{r}_i - \mathbf{r}_j|_{\perp}) \, \Theta(D - |z_i - z_j|) \right\rangle . \tag{32}$$

Here $\Theta(x)$ denotes the Heaviside step function and D is a small parameter ($D^* \approx 0.5$) defining what is meant in simulations by saying that molecules belong to the same plane normal to $\hat{\mathbf{z}}$. Note that regarding $\mathbf{r}_i$ and $\mathbf{r}_j$ in the Eq.(30) as positions of the dipole moments yields another interesting pair distribution function. It shows the tendency for the dipoles to gather in the plane.

In analogy to the case of longitudinal correlations (31), we can introduce transversal correlations $P_{\perp}^{(2)}(r_{\perp}, \uparrow\uparrow)$ and $P_{\perp}^{(2)}(r_{\perp}, \uparrow\downarrow)$, for parallel and antiparallel dipolar orientations, respectively, and $P_{\perp}^{(2)}(r_{\perp})$, for arbitrary orientation of the dipoles. Also, by expanding the general $g_{\perp}(\mathbf{r}_{\perp})$ into angular Fourier series we can introduce tetratic, hexatic *etc.* order parameters measuring the degree of angular correlations between the clusters of molecules. For example, the hexatic order is given by the hexatic order parameters $\Psi_{6n}(\overline{r}_{\perp})$ defined as

$$\begin{aligned} P_{\perp}^{(2)}(\mathbf{r}_{\perp}) &\equiv \frac{1}{2D} \sum_{s_1 s_2} \int_{-D}^{D} P^{(2)}(\mathbf{r}, s_1\hat{\mathbf{z}}, s_2\hat{\mathbf{z}}) \, \mathrm{d}z \\ &= P_{\perp}(\overline{r}_{\perp}) \sum_n \Psi_{6n}(\overline{r}_{\perp}) \, \exp\left(i \, 6n\phi_{jk}\right), \end{aligned} \tag{33}$$

where $\overline{r}_{\perp}$ is the average in-plane nearest neighbor separation (position of the leading peak of $g_{\perp}(r_{\perp})$) and ϕ_{jk} is the angle that the separation vector $\mathbf{r}_j - \mathbf{r}_k$ between neighboring molecules j and k makes with the x-axis. The dominant hexatic order parameter corresponds to $n = 1$ in the formula (33). In selecting the nearest neighbors we can consider molecules separated *e.g.* between $\overline{r}_{\perp} \pm \delta$ with δ being the distance from $\overline{r}_{\perp}$, where the magnitude of the leading peak of $g_{\perp}(r_{\perp})$ halves. For ideal triangular lattice $\Psi_6 = 1$.

5.3 Three-body distribution functions

Structural properties of a system could further be characterized using higher order distributions. Of them, the triplet distribution function is of particular importance, especially for strongly polar liquid crystals where frustration plays an important rôle [5–7]. Although correlations higher than two-body are straightforward to evaluate in simulations [77] the results for liquid crystals are scarce [48]. This is probably due to the fact that the general parametrization of the three-body distribution in terms of spherical invariants is quite

complicated and the calculation of averages time consuming. Even for a relatively small system of $N = 648$ IOGB molecules which we have studied the number of triplet configurations to be analyzed in one cycle is gigantic and equals $N(N-1)(N-2)/6 = 45\,139\,896$. Also visualization of the correlations, even if we manage to count triplets, is a nontrivial task.

For ideally oriented dipolar systems the task is manageable as the triplet distribution function $P^{(3)}$ considerably simplifies [48]. Actually, we are going to concentrate only on the translationally invariant part of the in plane three-body correlations which reads

$$P_{\perp}^{(3)}(r_{\perp},\theta,s_1s_2s_3) = \frac{V^2}{8\pi r_{\perp}^2 D^2 N^3}\Big\langle \sum_i \sum_{j\neq i} \sum_{k\neq j\neq i} \delta_{s_1s_i}\delta_{s_2s_j}\delta_{s_3s_k} \\ \delta(r_{\perp}-|\mathbf{r}_j+\mathbf{r}_i|_{\perp})\,\delta(r_{\perp}-|\mathbf{r}_k+\mathbf{r}_i|_{\perp})\,\Theta(D-|z_j-z_i|) \\ \Theta(D-|z_k-z_i|)\,\delta(\theta - Min(|\phi_j-\phi_k|, 2\pi-|\phi_j-\phi_k|))\Big\rangle. \tag{34}$$

By definition $P_{\perp}^{(3)}$ counts only those triplets that lie in planes perpendicular to the director and form isosceles triangles with two of the three sides being r and the angle between them being θ.

Owing to the symmetry of the IOGB model we think that other configurations do not contribute in an essential way to a quantitative understanding of the three-body correlations. As for the pair distribution two cases are considered. In the first case the vectors $\mathbf{r}_i$, $\mathbf{r}_j$, and $\mathbf{r}_k$ in (34) are assumed to refer to the centers of mass of the molecules. In the second case these vectors parameterize positions of the dipole moments. Thus $P_{\perp}^{(3)}$ accounts for tendency of the three centers of mass or, in the second case, of the three dipole moments to gather in planes perpendicular to the director.

Moreover we will distinguish three nonequivalent dipole configurations: $s_1s_2s_3 = \uparrow\uparrow\uparrow$, $\uparrow\uparrow\downarrow$ and $\uparrow\downarrow\downarrow$, and determine corresponding distribution functions $P_{\perp}^{(3)}(r_{\perp},\theta,\uparrow\uparrow\uparrow)$, $P_{\perp}^{(3)}(r_{\perp},\theta,\uparrow\uparrow\downarrow)$ and $P_{\perp}^{(3)}(r_{\perp},\theta,\uparrow\downarrow\downarrow)$, where the dipole moment s_1 refers to the nonequivalent vertex of isosceles triangles. Summing up over all possible orientations of $s_1s_2s_3$ yields the total distribution $P_{\perp}^{(3)}(r_{\perp},\theta)$. All technical details concerned with the calculations of $P_{\perp}^{(3)}$ are given in our publication [48].

6 Hard particles with dipoles

Zarragoicoechea and coworkers were the first to examine by means of computer simulations the effect of the dipole moment immersed into several hard body molecules (cut-spheres [83–85], ellipsoids of revolution [86], spherocylinders [85,87,88]) on phase equilibria. They concluded that the dipolar forces are of minor importance to the formation of mesogenic phases.

By re-examining the hard spherocylinder case McGrother and coworkers [62,89–92] only partly supported these observations. Their detailed simulations refer to the case of the spherocylinders with length to diameter ratio equal to 5, for which the system of vanishing dipole moment is well documented and exhibits isotropic, nematic and smectic A phases [75]. They found that central longitudinal dipole moments tend to destabilize the nematic phase relative to the isotropic and the smectic A phases as compared to the non-polar system. This is due to the strong enhancement of the molecular side-by-side in-plane antiparallel correlations which are responsible for the formation of the smectic layers. It is also found that an isotropic - nematic - smectic A triple point exists below which the nematic phase disappears.

The nematic phase is also destabilized relative to the smectic A phase (but not to the isotropic phase) for systems with a central transverse dipole moment. In this case the enhanced tendency to form layers is due to strong nose-to-tail interaction of the transverse dipoles. These interactions cause that the dipoles can form chain and ring domain structures within smectic layers. The terminal longitudinal dipoles, on the other hand, destabilize smectic A relative to nematic, where the latter phase becomes stable only at high densities.

7 Dipolar Gay-Berne systems

Although the dipolar interactions added to anisotropic repulsion yield an interesting model system with rich liquid crystalline phase behavior, the anisotropic attraction is by no means negligible in the stabilization of orientationally ordered phases. A model that takes all the three elements into account *i.e.* repulsion at short distances, dispersive interactions at large distances and dipolar forces is the Gay-Berne system with embedded dipole moments. Here we discuss the results of computer simulations for this model. The discussion is illustrated with our NVT Monte Carlo simulations for the IOGB system composed of $N = 648$ polar molecules with longitudinal dipole moments (some tests being performed for $N = 2592$) [48]. The dipolar energy is calculated with the help of both, Ewald summation technique and reaction field. We investigate the influence of the dipole strength and the dipole location in the molecule on the formation of the smectic A phase and of higher ordered phases. Studied are also dipolar correlations in these phases.

7.1 Central dipole moments

For central, longitudinal dipole moments ($d^* = 0$) Satoh *et al.* [38] have shown that the isotropic liquid - nematic phase transition is not sensitive to the value of the dipole moment. Contrary to that the nematic-smectic A phase transition is shown to depend on the strength of the dipole moment. Moreover the stability range of the smectic phase for strong dipoles is wider compared

to that in nonpolar systems. That is the central dipole moments enhance stability of smectic layers, which agrees qualitatively with what is reported for dipolar hard spherocylinders. Similar conclusions can be drawn for the IOGB model. We illustrate this with simulations performed for $T^* = 2.8$ and $\rho^* = 0.335$. Starting from the nematic reference state we find that an increase of the central dipole moment from $\mu^* = 0$ to $\mu^* = 1.5$ (the average dipole-dipole energy $< V_{dd} > / < V >$ being 23% of the total energy) yields a (weak) dipole-induced smectic A structure. The structure is characterized by $\tau_2 = 0.11$ ($\zeta_{2n+1} = 0$), and the layer spacing, $l^* \approx 2.7$, indicating that the layers are slightly interdigitated.

The pair distributions, Figs. (7a) and (7b), are fluid-like and similar to what is observed in the nematic phase. As deduced from Figs. (7a) and (7b)

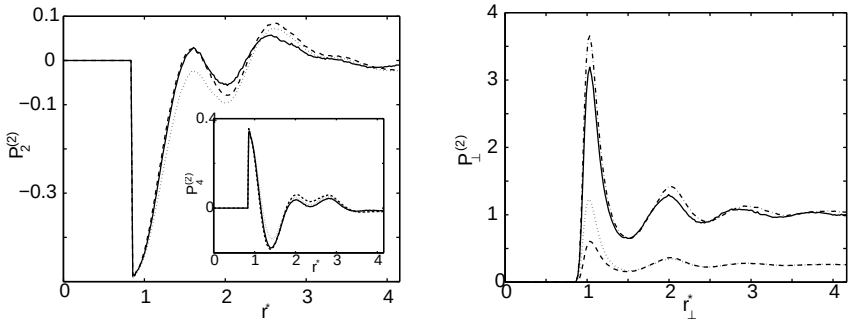

(**a**) (**b**)

Fig. 7. (**a**) The pair distribution functions $P_L^{(2)}(r^*)$ for $L = 2$ and $L = 4$ (inset) in the nematic phase of nonpolar molecules (continuous line) and $P_L^{(2)}(r^*, s_1 s_2)$ in the smectic A phase of the IOGB model with central dipole moment $\mu^* = 1.5$. The dotted line represents the $s_1 s_2 = \uparrow\downarrow$ while the dashed one corresponds to $s_1 s_2 = \uparrow\uparrow$ dipole configurations. (**b**)The transversal pair distribution functions $P_\perp^{(2)}(r_\perp^*)$ for the same cases as in (a). Additionally, the dash-dotted line represents the total distribution function, $P_\perp^{(2)}(r_\perp^*)$

the dipoles are distributed randomly within the layers, with no track of long-range ordering. The short-range, in-plane correlations are dominated by the antiparallel molecular arrangement (Fig. (7b)). The 'fine structure' of these correlations, as displayed by the triplet in-plane distribution function, shows local hexagonal structure and linear correlations of the triplets. The leading peak of these correlations is dominated by the triplets occupying equilateral triangles as seen from Figs. (8a) and (8b). Figures (8a) and (8b) also show that the peak at 60° is due to the triplets with one dipole moment being oriented in the opposite direction than the other two. The contribution from linear triplets, where the middle dipole has different orientation than the terminal ones, is equally important (see peak at 180° in Fig. (8b)). The

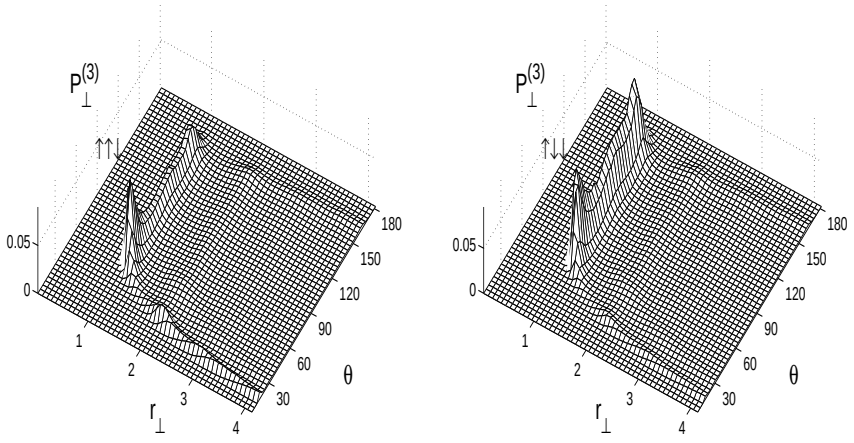

(**a**) (**b**)

Fig. 8. The triplet distribution function $P_{\perp}^{(3)}(r_{\perp}^{*}, \theta, s_1 s_2 s_3)$ for the IOGB model with central dipole moments of $\mu^{*} = 1.5$ in the smectic A phase: (**a**) $s_1 s_2 s_3 = \uparrow\uparrow\downarrow$; (**b**)$s_1 s_2 s_3 = \uparrow\downarrow\downarrow$

distribution function where all three dipoles are oriented in the same direction is negligible.

Further increase of magnitude of the central dipole to $\mu^{*} = 2.0$ ($< V_{dd} > / < V > \approx 37\%$) leads to a new structure which, most likely, is a crystalline S_B with ABAB stacking. Again no long-range dipolar order across the layers (Fig. (9a)) or within the layers is observed even though the smectic order parameter τ_2 of 0.8 is close to its saturation value of 1. Inspection of $P_{\perp}^{(2)}$ (Fig. (9b)) shows that the system has developed hexagonal type of correlations with the hexatic order parameter Ψ_6, Eq.(33), of 0.69. The hexagonal in-plane arrangement becomes even more apparent by looking at the triplet correlations. They follow the same trends as previously observed ones for $\mu^{*} = 1.5$ with one exception that the corresponding peaks are now much better resolved and with higher amplitudes. A similar structure also exists for an even higher central dipole moment ($\mu^{*} = 2.5$) or lower temperatures. This is in line with the very recent MC NPT simulations by Houssa *et al.* [63], who also observe a stable dipolar S_B phase, most probably of AA or AB stacking, although this aspect of the ordering has not been studied.

Simulations of Houssa *et al.* [63] additionally allow interesting conclusions to be drawn about the stability of the nematic phase. Namely they show that for sufficiently strong dipole moments ($\mu^{*} = 2.5$) added to the OGB potential the nematic phase could be eliminated forcing the system to evolve directly from the isotropic phase to smectic B phase. Again most of the results obtained for the dipolar Gay-Berne systems are in qualitative agreement with those of equivalent dipolar hard spherocylinders.

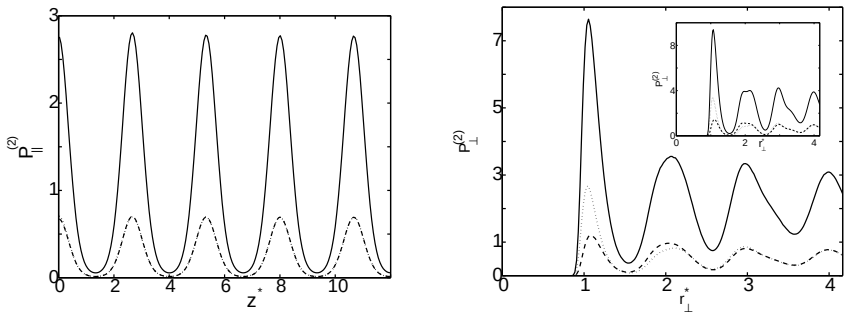

(**a**) (**b**)

Fig. 9. (**a**)The axial pair distribution function $P_{||}^{(2)}(z^*, s_1 s_2)$ and (**b**) the transversal pair distribution function, $P_{\perp}^{(2)}(r_{\perp}^*, s_1 s_2)$ in the smectic B phase. The dipolar strength of the central dipole is $\mu^* = 2$. The solid lines represent dipole-averaged total distribution functions and the dashed lines are for the $s_1 s_2 = \uparrow\uparrow$ distribution. The dotted lines give the $s_1 s_2 = \uparrow\downarrow$ distributions. The inset in (b) shows the transversal distribution in the same phase, but for $T^* = 2$

Central dipole moments perpendicular to the long molecular axis of the OGB molecules also have been considered [41,46], and the results appear somewhat controversial. Namely in the paper [41] the dipoles were found to have no impact on the liquid crystalline transitions, in contrast to an equivalent hard spherocylinders system, where transverse dipoles enhance the stability of the smectic A phase [90]. On the other hand, similar studies performed by Berardi *et al.* [46] demonstrate enhanced layering and formation of chains and rings of dipoles in smectic planes, consistent with the results for dipolar hard spherocylinders [90]. One possible explanation of this discrepancy is that in the paper [41] the long-range dipole-dipole interactions have been treated in the same way as the Gay-Berne part, *i.e.* without referring to the Ewald- or reaction field methods.

7.2 Intermediate and terminal dipole moments

Simulations with noncentral locations of the dipole moments also were performed. In particular, terminal longitudinal dipoles were studied by Satoh *et al.* [39]. They found that the isotropic liquid - nematic transition temperature is shifted towards higher temperatures and the temperature range of the stability of the nematic phase is enhanced with increasing value of the dipole moment. Additionally, the strong terminal dipoles form at low temperatures a crystalline structure with tetragonal order within layers [42]. Berardi *et al.* [40] concentrated on the smectic phases and they found smectic $\tilde{A}$ phase for the OGB system with terminal dipoles.

Simulations carried out for the equivalent IOGB model are consistent with those findings although our system was too small to observe modulated anti-

ferroelectric bilayer stripe domains characteristic of smectic $\tilde{A}$. Two cases were considered: *(a)* nearly terminal dipoles ($d^* = 0.75$) and *(b)* the dipoles localized at molecular end ($d^* = 1$).

One of the structures found for $d^* \approx 0.75$ and for moderate dipole moments ($\mu^* \approx 1.5$) is, with high probability, the smectic A_d. Such identification is supported by the small value of the translational order parameter τ_2 ($\tau_2 \approx 0.35$) and by properties of the correlation functions. Indeed, we observe that the relative distance between the positions of the molecular centers along the z direction is about 1.7, which means that the layers are strongly interdigitated. Analysis of transversal distributions of the molecules within a single layer and within the planes of the dipole moments additionally shows that the strongest transversal pair correlations (and hence also the triplet ones) are for in-plane antiparallel dipole moments with the corresponding centers of mass of the molecules being separated by $l \approx 1.7$ (*see* Figs.(10a) and (10b)). The leading peak of $P_\perp^{(2)}$ at $r_\perp^* \approx 0.9$, Fig.(10a) comes from molecular pairs

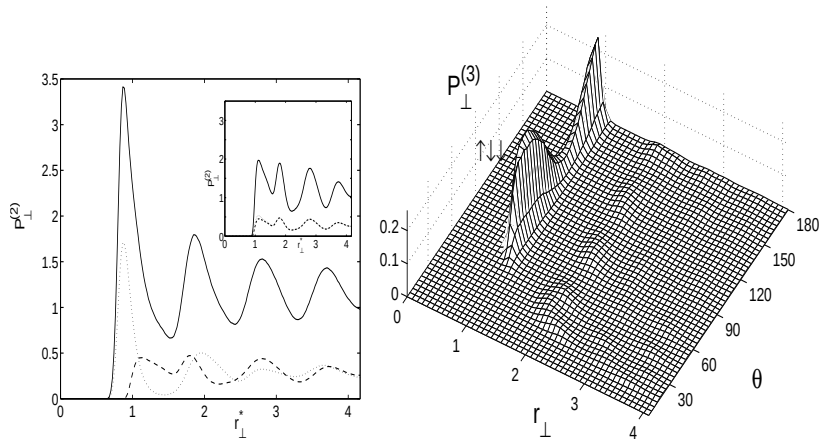

(**a**) (**b**)

Fig. 10. (**a**) The transversal pair distribution function, $P_\perp^{(2)}(r_\perp^*, s_1 s_2)$ for the in-plane dipole moments, in the smectic A_d phase of the IOGB model. The dipole moment μ^* of 1.5 is located at $d^* = 0.75$. The molecular centers are localized in the neighboring layers. The continuous line represents the total distribution function, $P_\perp^{(2)}(r_\perp^*)$; dotted and dashed lines correspond to $s_1 s_2 = \uparrow\downarrow$ and $s_1 s_2 = \uparrow\uparrow$, respectively. The inset shows the corresponding transversal distribution viewed from smectic plane of molecular centers. (**b**) The triplet distribution function $P_\perp^{(3)}(r_\perp^*, \theta, s_1 s_2 s_3)$ for the case (a) in the plane of $\uparrow\downarrow\downarrow$-oriented dipole moments (the centers of mass of the molecules with oppositely oriented dipoles are located in the neighboring layers). This case shows the strongest dipolar correlations between the dipoles

that compensate their dipole moments (*weak dimers*) and is much stronger than the peak at $r_{\perp}^{*} \approx 1.06$ of the in-layer correlations (inset in Fig. (10a)). The total triplet dipole correlations, calculated in the plane of the dipoles, are practically dominated by the $s_1 s_2 s_3 = \uparrow\downarrow\downarrow$ triplet correlations, which we show in Fig. (10b). These correlations have essentially two broad peaks at 90° and 180°. Although this phase could also be a crystalline phase with interdigitated, tetragonal layers (S_{crT}) the apparently very small probability to have in-plane molecules with parallel dipole moments at reduced distance of $0.9 \times \sqrt{2}$ suggests that the structure is more likely of smectic A_d-type. The smectic layers could be viewed as being supported by correlated dimers with the layer spacing $2l^*$ of approximately 3.4. Interestingly, the local hexagonal ordering of central dipoles is transformed into a tetragonal one.

For dipole moments of magnitude $\mu^* = 2$ the peaks of the distribution functions become sharper and their fine structure could be resolved indicating that the structure is of S_{crT} type, similar to that reported by Satoh [42]. But even now with relatively strong dipolar interactions, no long-range dipolar order has been found. We observe, however, a strong enhancement of the $\uparrow\uparrow\uparrow$ triplet correlations indicating that for stronger dipoles we should detect a crystalline phase with polarized layers. Indeed, for very strong dipoles ($\mu^* = 2.5$) a bilayer crystalline structure with tetragonal in-plane ordering is stabilized. Now both order parameters ζ_1 and τ_2 are nonzero and high ($\zeta_1 = 0.89$, $\tau_2 = 0.75$), which indicates that the antiferroelectric dipolar order is even stronger than the smectic ordering. The crystalline structure thus has dipolar ordering similar to that observed for the antiferroelectric smectic A_2 phase. Interestingly, the axial *up–up* correlations are stronger than the *up–down* correlations. The *up–down* correlations within one smectic layer are almost negligible.

For large shifts in the dipole location ($d^* = 1$) and for $\mu^* = 2$ we recovered planar domains very similar to those reported by Berardi *et al.* [40], but present systems were too small for a quantitative analysis of the ordering.

8 Towards realistic simulations

Computer simulations based on detailed atomistic interactions between liquid crystalline molecules are still quite rare (*see e.g.* [27,93,94] and references therein). The reason for that is the computational complexity of interactions, which causes that only small systems are manageable so far (up to 144 molecules). Consequently, studies are restricted to the isotropic, nematic and, sometimes, crystalline phases for which the system size is not a severe obstacle.

As concerning simulations of realistic polar liquid crystals the molecular systems considered so far were those with terminal dipoles (PCH5, PCH5-Cl, 5CB, 5OCB). Of these the most accurate atomistic studies are by Cook and Wilson [27]. Their comparison with experiment of densities and of dipolar

properties of PCH5 and PCH5-Cl molecules in the isotropic phase is quite encouraging. It shows that atomistic simulations indeed may have predictive power for bulk properties of mesogens. We expect that within the next few years a determination of liquid crystalline behavior from molecular modelling prior to synthesis should be possible.

Acknowledgments

This work was supported by the Polish project (KBN) No. 5 P03B 052 20 and by the project C12 of Collaborative Research Centre 382 of the Deutsche Forschungsgemeinschaft (DFG).

References

1. P. G. de Gennes and J. Prost: *The Physics of Liquid Crystals*, 2nd edn. (Clarendon Press, Oxford 1993)
2. G. W. Gray and J. W. Goodby: *Smectic liquid crystals. Textures and structures*, (Leonard Hill, Glasgow 1984)
3. G. W. Gray, K. J. Harrison, and J. A. Nash, Electron. Lett. **37**, 18 (1973)
4. G. W. Gray and J. E. Lydon, Nature **252**, 221 (1974)
5. P. E. Cladis, Phys. Rev. Lett. **35**, 48 (1981)
6. A. N. Berker and J. S. Walker, Phys. Rev. Lett. **4**7, 1469 (1981)
7. L. Longa and W. H. de Jeu, Phys. Rev. **A** 26, 1632 (1982)
8. L. Longa, *"Models of high-temperature liquid crystalline phases and of related phase transitions"*, Institute of Nuclear Physics, Kraków, Raport No 1454/PH (1989)
9. A. M. Levelut, R. J. Tarento, F. Hardouin, M. F. Achard, and G. Sigaud, Phys. Rev. **A 24**, 2180 (1981)
10. F. Hardouin, A. M. Levelut, M. F. Achard, and G. Sigaud, J. Chim. Phys. **80**, 53 (1983)
11. L. Longa and W. H. de Jeu, Phys. Rev. **A** 28, 2380 (1983)
12. Y. Matsunaga, and S. Miyamoto, Mol. Cryst. Liq. Cryst. **237**, 311 (1993)
13. H. Matsuzaki, and Y. Matsunaga, Liq. Cryst. **14**, 105 (1993)
14. G. Pelzl, S. Diele, and W. Weissflog, Adv. Mater. **11**, 707 (1999)
15. M. P. Allen, D. J. Tildesley, *Computer Simulation of Liquids*, (Clarendon Press, Oxford 1987)
16. D. Frenkel and B. Smit, *Understanding molecular simulation: from algorithms to applications*,2nd Ed. (Academic Press, San Diego 2001)
17. F. Biscarini, C. Zannoni, C. Chiccoli, and P. Pasini, Mol. Phys. **73**, 439 (1991)
18. R. Berardi, M. Ricci, and C. Zannoni, CHEMPHYSCHEM **7**, 444 (2001)
19. T. Watanabe, S. Miyata, T. Furukawa, H. Takezoe, T. Nishi, M. Sone, A. Migita, and J. Watanabe, Jpn. J. Appl. Phys. **35**, L505 (1996)
20. S.I. Stupp, V. LeBonheur, K. Walker, L.S. Li, K.E. Huggins, M. Keser, and A. Amstutz, Science **276**, 384 (1997)
21. T. Niori, T. Sekine, J. Watanabe, T. Furukawa, and H. Takezoe, J. Mater. Chem. **6**, 1231 (1996)
22. J. J. Weis, D. Levesque, and G. J. Zarragoicoechea, Phys. Rev. Lett. **69**, 913 (1992)

23. R. Berardi, S. Orlandi, and C. Zannoni, J. Chem. Soc., Faraday Trans. **93**, 1493 (1997)
24. S. Singh, Phys. Reports. **324**, 107 (2000)
25. L. M. Blinov, Liq. Cryst. **24**, 143 (1998)
26. A. J. Stone, in *The Molecular Physics of Liquid Crystals*, edited by G. R. Luckhurst and G. W. Gray (Academic Press, London 1981)
27. M. J. Cook and M. R. Wilson, Liq. Cryst. **27**, 1573 (2000)
28. J. G. Gay and B. J. Berne, J. Chem. Phys. **7**4, 3316 (1981)
29. E. de Miguel, L. F. Rull, M. K. Chalam, and K. E. Gubbins, Mol. Phys. **7**1, 1223 (1990)
30. E. de Miguel, L. F. Rull, M. K. Chalam, K. E. Gubbins and F. van Swol, Mol. Phys. **7**2, 593 (1991)
31. E. de Miguel, L. F. Rull, M. K. Chalam, and K. E. Gubbins, Mol. Phys. **7**4, 405 (1991)
32. M. A. Bates and G. R. Luckhurst, J. Chem. Phys. **1**10, 7087 (1999)
33. J. T. Brown, M. P. Allen, E. M. del Río, and E. de Miguel, Phys. Rev. E **5**7, 6685 (1998)
34. R. Berardi, C. Fava, and C. Zannoni, Chem. Phys. Lett. **2**36, 462 (1995)
35. R. Berardi and C. Zannoni, J. Chem. Phys. **1**13, 5971 (2000)
36. G. La Penna, D. Catalino, and C. A. Veracini, J. Chem. Phys. **1**05, 7097 (1996)
37. M. P. Neal, A. J. Parker, and C. M. Care, Mol. Phys. **9**1, 603 (1997)
38. K. Satoh, S. Mita, and S. Kondo, Liq. Cryst. **2**0, 757 (1996)
39. K. Satoh, S. Mita, and S. Kondo, Chem. Phys. Lett. **2**55, 99 (1996)
40. R. Berardi, S. Orlandi, and C. Zannoni, Chem. Phys. Lett. **2**61, 357 (1996)
41. E. Gwóźdź, A. Bródka, and K. Pasterny, Chem. Phys. Lett. **2**67, 557 (1997)
42. K. Satoh, S. Mita, and S. Kondo, Mol. Cryst. Liq. Cryst. **3**00, 143 (1997)
43. G. Ayton, D. Q. Wei, and G. N. Patey, Phys. Rev. E **5**5, 447 (1997)
44. R. Berardi, S. Orlandi, and C. Zannoni, J. Chem. Soc., Faraday. Trans. **9**3, 1493 (1997)
45. M. Houssa, L. F. Rull, and S. C. McGrother J. Chem. Phys. **1**09, 9529 (1998)
46. R. Berardi, S. Orlandi, and C. Zannoni, Int. J. Mod. Phys. C **1**0, 477 (1999)
47. G. Cholewiak, J. Stelzer and L. Longa, SPIE Int. Soc. Opt. Eng. **3**318, 179 (1998)
48. L. Longa, G. Cholewiak, and J. Stelzer, A. Phys. Pol. B **3**1, 801 (2000)
49. G. Cholewiak, PhD Thesis, (Jagellonian University, M. Smoluchowski Institute of Physics, Kraków 2002)
50. I. M. Withers, C. M. Care, and D. J. Cleaver J. Chem. Phys. **1**13, 5078 (2000)
51. W. L. Wagner, Mol. Cryst. Liq.Cryst. **2**99, 33 (1997)
52. W. L. Wagner and L. Bennett Mol. Phys. **9**4, 571 (1998)
53. S. C. McGrother and G. Jackson, Phys. Rev. Lett. **7**6, 4183 (1996)
54. S. W. de Leeuw, J. W. Perram, E. R. Smith, Proc. R. Soc. Lond. A, **3**73, 27 (1980)
55. J. W. Perram, H. G. Petersen, S. W. de Leeuw, Mol. Phys. **6**5, 875 (1988)
56. M. Sprik, in *Observation, Prediction and Simulation of Phase Transitions in Complex Fluids*, edited by M. Baus, L. F. Rull and J. P. Ryckaert (Kluwer, Dortrecht 1995)
57. V. Lobaskin and P. Linse, J. Chem. Phys., **1**09, 3530 (1998)
58. M. Neumann and O. Steinhauser, Chem. Phys. Lett., **9**5, 417 (1983)
59. J. Kolafa and J. W. Perram, Mol. Simul., **9**, 351 (1992)

60. D. Fincham, Mol. Simul., **1**3, 1 (1994)
61. G. Hummer Chem. Phys. Lett., **2**35, 297 (1995)
62. A. Gil-Villegas, S. C. McGrother and G. Jackson, Mol. Phys. **9**2, 723 (1997)
63. M. Houssa, A. Qualid, and L. F. Rull, Mol. Phys. **9**4, 439 (1998)
64. T. M. Nymand and P. Linse, J. Chem. Phys. **1**12, 6152 (2000)
65. L. Onsager, J. Am. Chem. Soc. **5**8, 1486 (1936)
66. J. A. Barker and O. R. Watts, Chem. Phys. Lett., **3**, 144 (1969)
67. I. G. Tironi, R. Sperb, P. E. Smith, and W. F. van Gunsteren, J. Chem. Phys., **1**02, 5451 (1995)
68. P. H. Hünenberger and W. F. van Gunsteren, J. Chem. Phys., **1**08, 6117 (1998)
69. S. L. Marshall, J. Phys.: Cond. Mat., **1**2, 4575 (2000)
70. P. Demontis, S. Spanu, and G. B. Suffritti, J. Chem. Phys., **1**14, 7980 (2001)
71. J. J. Weis and D. Levesque, Phys. Rev.E, **4**8, 3728 (1993)
72. J. E. Roberts and J. Schnitker, J. Chem. Phys., **1**01, 5024 (1994)
73. J. E. Roberts and J. Schnitker, J. Phys. Chem., **9**9, 1322 (1995)
74. B. Garzón, S. Lago, and C. Vega, Chem. Phys. Lett., **2**31, 366 (1994)
75. P. Bolhuis and D. Frenkel, J. Chem. Phys., **1**06, 666 (1997)
76. C. Zannoni, in *The Molecular Physics of Liquid Crystals*, edited by G. R. Luckhurst and G. W. Gray (Academic Press, London 1981)
77. J. P. Hansen and I. R. McDonald *Theory of Simple Liquids* 2^{nd} edition, (Academic Press, London 1986)
78. J. P. Hansen, in *Observation, Prediction and Simulation of Phase Transitions in Complex Fluids*, edited by M. Baus, L. F. Rull and J. P. Ryckaert (Kluwer, Dortrecht 1995)
79. A. Lindner, in *Drehimpulse in der Quantenmechanik*, (B. G. Teubner, Stuttgart 1984)
80. J. Vieillard-Baron, Mol.Phys., 28, 809 (1974)
81. P. J. Wojtowicz, in *Introduction to Liquid Crystals*, edited by E. B. Priestley, P. J. Wojtowicz, and P. Sheng (Plenum Press, New York and London 1975)
82. L. Longa, G. Cholewiak, H.-R. Trebin, and G. R. Luckhurst, Eur. Jour. Phys. E **4**, 51 (2001)
83. G. Z. Zarragoicoechea, D. Levesque, and J. J. Weis, Mol. Phys. **7**4, 629 (1991)
84. G. Z. Zarragoicoechea, D. Levesque, and J. J. Weis, Mol. Phys. **7**5, 989 (1992)
85. J. J. Weis, D. Levesque, and G. J. Zarragoicoechea, Phys. Rev. Lett., **69**, 913 (1992)
86. J. J. Weis, D. Levesque, and G. J. Zarragoicoechea, Phys. Rev. A, **46**, 7783 (1992)
87. D. Levesque, J. J. Weis, and G. Z. Zarragoicoechea, Phys. Rev. **E** 47, 496 (1993)
88. G. Z. Zarragoicoechea, D. Levesque, and J. J. Weis, Mol. Phys. **7**8, 1475 (1993)
89. S. C. McGrother, A. Gil-Villegas, and G. Jackson, J. Phys. Cond. Matt. **8**, 9649 (1996)
90. A. Gil-Villegas, S. C. McGrother, and G. Jackson, Chem. Phys. Lett. **2**69, 441 (1997)
91. S. C. McGrother, G. Jackson, and D. J. Photinos, Mol. Phys. **9**1, 751 (1997)
92. S. C. McGrother, A. Gil-Villegas, and G. Jackson, Mol. Phys. **9**5, 657 (1998)
93. S. Hauptmann, T. Mosell, S. Reiling, and J. Brickmann, Chem. Phys., **2**08, 57 (1996)
94. B. Stevensson, A. V. Komolkin, D. Sandström, and A. Maliniak, J. Chem. Phys., **1**14, 2332 (2001)